Eur J Nucl Med Mol Imaging (2015) 42:1976–1983
DOI 10.1007/s00259-015-3125-3

ORIGINAL ARTICLE

Pre-therapeutic dosimetry of normal organs and tissues of ^{177}Lu-PSMA-617 prostate-specific membrane antigen (PSMA) inhibitor in patients with castration-resistant prostate cancer

Levent Kabasakal[1] · Mohammad AbuQbeitah[1] · Aslan Aygün[1] · Nami Yeyin[1] · Meltem Ocak[2] · Emre Demirci[3] · Turkay Toklu[4]

Received: 27 April 2015 / Accepted: 29 June 2015 / Published online: 31 July 2015

Abstract
Purpose ^{177}Lu-617-prostate-specific membrane antigen (PSMA) ligand seems to be a promising tracer for radionuclide therapy of progressive prostate cancer. However, there are no published data regarding the radiation dose given to the normal tissues. The aim of the present study was to estimate the pretreatment radiation doses in patients who will undergo radiometabolic therapy using a tracer amount of ^{177}Lu-labeled PSMA ligand.
Methods The study included seven patients with progressive prostate cancer with a mean age of 63.9±3.9 years. All patients had prior PSMA positron emission tomography (PET) imaging and had intense tracer uptake at the lesions. The injected ^{177}Lu-PSMA-617 activity ranged from 185 to 210 MBq with a mean of 192.6±11.0 MBq. To evaluate bone marrow absorbed dose 2-cc blood samples were withdrawn in short variable times (3, 15, 30, 60, and 180 min and 24, 48, and 120 h) after injection. Whole-body images were obtained at 4, 24, 48, and 120 h post-injection (p.i.). The geometric mean of anterior and posterior counts was determined through region of interest (ROI) analysis. Attenuation correction was applied using PSMA PET/CT images. The OLINDA/EXM dosimetry program was used for curve fitting, residence time calculation, and absorbed dose calculations.
Results The calculated radiation-absorbed doses for each organ showed substantial variation. The highest radiation estimated doses were calculated for parotid glands and kidneys. Calculated radiation-absorbed doses per megabecquerel were 1.17±0.31 mGy for parotid glands and 0.88±0.40 mGy for kidneys. The radiation dose given to the bone marrow was significantly lower than those of kidney and parotid glands ($p<0.05$). The calculated radiation dose to bone marrow was 0.03±0.01 mGy/MBq.
Conclusion Our first results suggested that ^{177}Lu-PSMA-617 therapy seems to be a safe method. The dose-limiting organ seems to be the parotid glands rather than kidneys and bone marrow. The lesion radiation doses are within acceptable ranges; however, there is a substantial individual variance so patient dosimetry seems to be mandatory.

Keywords Prostate cancer · Radionuclide treatment · Prostate specific membrane antigen · PSMA · Lu-177-PSMA · Castration resistant · Radiometabolic therapy

Introduction

Prostate-specific membrane antigen (PSMA) is a type II membrane glycoprotein highly expressed by all prostate cancers and the expression increases with tumor aggressiveness, metastatic disease, and disease recurrence [1–3]. The unique expression of PSMA provides an excellent target for prostate cancer imaging and therapy using ^{68}Ga- and ^{177}Lu-labeled ligands. Glu-NH-CO-NH-Lys-[Ga-68-(HBED-CC)] (^{68}Ga-PSMA-11) has been suggested as a novel tracer that can detect prostate cancer relapses and metastases with high contrast by targeting the PSMA [4–8]. Also its counterpart ^{177}Lu-PSMA-

✉ Levent Kabasakal
lkabasakal@tsnm.org

[1] Department of Nuclear Medicine, Cerrahpasa Medical Faculty, Istanbul University, Istanbul, Turkey

[2] Department of Pharmaceutical Technology, Pharmacy Faculty, Istanbul University, Istanbul, Turkey

[3] Department of Nuclear Medicine, Sisli Etfal Training and Research Hospital, Istanbul, Turkey

[4] Department of Nuclear Medicine, Yeditepe University Medical Faculty, Istanbul, Turkey

617 seems to be a promising novel tracer for systemic radionuclide therapy in patients with castration-resistant prostate cancer [9, 10].

The basic principle of radionuclide therapy is to give a maximum justifiable dose that does not cause serious toxicity in order to get an effective antitumor effect. The dose-limiting organs for this type of therapy are the kidneys, parotid glands, and the bone marrow. In order to avoid toxicity the amount of radiation dose given to these dose-limiting organs has to be estimated. However, there are no published data regarding the radiation-absorbed dose given to the normal tissues for systemic therapy with ^{177}Lu-PSMA-617.

Therefore, we aimed a pilot study to estimate radiation-absorbed doses to dose-limiting organs in order to develop a treatment plan for systemic therapy with ^{177}Lu-PSMA-617 in patients with castration-resistant prostate cancer.

Materials and methods

Patients

For this purpose seven patients were included in the study. All patients had histopathological diagnosis of prostate cancer. The ages ranged from 57 to 70 years (mean 63.9±3.9 years). Patients had prostatic surgery (n=3) and radiation therapy (n=4). All patients had hormonal therapy and had increasing blood PSA levels. The Gleason score was 9 in three patients, 8 in three patients, and 7 in one patient. Blood PSA levels ranged from 19 to 235 ng/ml (mean 85.43±74.46 ng/ml) (Table 1.). The study was approved by the local Ethics Committee.

PSMA PET/CT imaging

In order to decide eligibility for ^{177}Lu-PSMA-617 treatment, all patients had PSMA positron emission tomography (PET)/CT imaging using ^{68}Ga-PSMA-11. Radiolabeling was done with a fully automated radiopharmaceutical synthesis device based on a modular concept (Eckert & Ziegler Eurotope, Berlin, Germany). Briefly, a TiO2-based commercially available ^{68}Ge/^{68}Ga generator (Eckert & Ziegler Eurotope, Berlin, Germany) was eluted with 0.1 N hydrochloric acid (HCl), and a 1.2-ml fraction was added to 5 nmol of PSMA-11 (ABX GmbH, Radeberg, Germany); pH was adjusted to 3.5–4.0 by adding 1 mol/l sodium acetate solution. The reaction was done at room temperature for 120 s. The reaction solution was passed over a C18 cartridge (Sep-Pak, Waters, Milford, MA, USA), washed with saline, and finally eluted with 0.6 ml 50 % ethanol, which was followed by saline through a 0.22-μm sterile Millipore filter. Radiochemical purity, as determined by high-performance liquid chromatography (HPLC), exceeded 95 % in all cases. After the preparation and quality control of the radiotracers, all patients received 75–150 MBq of ^{68}Ga-PSMA-11 intravenously. Whole-body images were acquired 45–60 min post-injection (p.i.) of radiotracer using an integrated PET/CT scanner, which consisted of a full-ring high-resolution LSO PET and a six-slice CT (Siemens Biograph 6, Knoxville, TN, USA). Lesion uptake in PSMA PET/CT imaging was scored in three categories according to liver uptake: 1=lower than, 2=equal to, and 3=higher than liver uptake. Patients with lesions showing uptake equal to or higher than liver uptake were considered as candidates for ^{177}Lu-PSMA-617 therapy.

Preparation of ^{177}Lu-PSMA-617

The radiolabeling of PSMA-617 [10] was performed in a hot cell using ^{177}Lu Cl_3 (47 MBq/nmol of ligand) in 0.05 mol l^{-1} HCl (PerkinElmer, Waltham, MA, USA) with sodium ascorbate buffer pH 4.5 (Polatom, Otwock-Swierk, Poland) at 95 °C for 15 min. After cooling down of the reaction vial to room temperature, the volume was adjusted to 2 ml with saline, and 0.5–1.0 ml of sterile diethylenetriaminepentaacetic acid (DTPA) solution (3 mg ml^{-1} DTPA in saline) was added. After sterile filtration of this preparation to a sterile vial, the volume was completed until 20 ml with sterile saline under aseptic conditions. Radiochemical purity was determined by instant thin-layer chromatography silica gel (ITLC-SG) and radio-HPLC and was found to be≥98 %.

^{177}Lu-PSMA-617 imaging

The injected ^{177}Lu-PSMA-617 activity ranged from 185 to 210 MBq (4–4.6 nmol of the ligand) with a mean of 192.6± 11.0 MBq (4.1±0.2 nmol of the ligand). Anterior and posterior whole-body scans (WBS) were obtained at a scan speed of 10 cm/min using a dual-head gamma camera equipped with a medium-energy parallel-hole collimator (Symbia T16, Siemens, Erlangen, Germany). Double peak at 113 and 208 keV and 15 % window settings were used for WBS acquisition.

Dosimetry

For estimating the individual patient doses for source organs, which are right kidney, left kidney, and liver, and dose_limiting organs, which are bone marrow and parotid gland, anterior and posterior WBS were obtained and a conjugate view approach was used for determination of the absolute activity after definition of regions of interest (ROIs) for corresponding source region. An ROI was drawn over the contour of the organ and then reflected to the corresponding area in the other view.

The injected ^{177}Lu-PSMA-617 activity ranged from 185 to 210 MBq with a mean of 192.6±11.0 MBq. Due to the small

Table 1 Calculated radiation-absorbed doses (mGy/MBq ^{177}Lu-PSMA-617) of organs of each patient

Patient	Age	GS	PSA (ng/ml)	Parotid gland	Kidney	Bone marrow	Liver	Total body	Residence time (h)
1	65	8	48	1.66	0.76	0.025	0.27	0.049	24.6
2	62	9	110	0.96	1.66	0.048	0.46	0.094	46.3
3	57	8	19	0.94	0.98	0.037	0.23	0.058	49.4
4	65	7	89	1.48	0.52	0.021	0.25	0.035	27.6
5	63	9	235	1.07	0.69	0.058	0.34	0.098	62.0
6	65	9	78	1.25	1.03	0.030	0.22	0.057	26.5
7	70	8	19	0.80	0.51	0.022	0.18	0.036	28.7
Mean	63.9	8.3	85.4	1.17	0.88	0.034	0.28	0.061	37.9
SD	3.9	0.8	74.5	0.31	0.40	0.014	0.09	0.026	14.6

GS Gleason score, *PSA* prostate-specific antigen

quantity of injected tracer activity, WBS were obtained at different time points: 4, 24, 48, and 120 h p.i. Blood samples at 3, 10, 20, 40, 60, and 90 min and at 2, 3, 24, 48, and 72 h after ^{177}Lu-PSMA-617 infusion were obtained and 0.5 ml whole blood samples were counted in a well counter calibrated for ^{177}Lu.

In order to convert counts obtained from ROIs on WBS to activity, a gamma camera system calibration factor was defined by counting a known activity with different acquisition speeds taking into consideration a standardized geometry in air relative to the scintillation camera and using similar camera acquisition settings. Three different amounts of ^{177}Lu activities, 11.1 MBq/5 cc, 208.3 MBq/500 cc, and 94.0 MBq/102 cc, in different geometric shapes placed in different water-filled phantoms were scanned at three different acquisition speeds,. 5 cm/min, 10 cm/min, and 15 cm/min. Quantification of the phantoms to identify source activity was performed by the same person responsible for calculating the dosimetry. It was achieved by drawing ROIs over the images of the phantoms to obtain the corresponding counts necessary to initiate linear interpolation between imaging speeds. The function (y=−ax+b) (a.b: constants) generated from the linear fitting consequently was used to find the calibration factor in which X is equal to desired acquisition speed (10 cm/min) with a duration of 23 min for all patients. The source organ activity in a particular time was determined as it is described in Eqs. 1, 2, 3, and 4 of MIRD pamphlet no. 16 [11]:

$$A_j = \sqrt{\frac{IAIP}{e^{-\mu et}}}\frac{fj}{C} \tag{1}$$

$$fj = \frac{\left(\frac{\mu jtj}{2}\right)}{sinh\left(\frac{\mu jtj}{2}\right)} \tag{2}$$

$$\mu e = \left(\frac{1}{t}\right)\sum\nolimits_{i=1}^{n}(\mu iti - \mu j) + \left(\frac{1}{t}\right)\sum\nolimits_{i=1}^{n}(\mu i - \mu j)\,ti \tag{3}$$

$$F = \left\{\left[1-\left(\frac{IADJ}{IA}\right)\left(1-\frac{tj}{t}\right)\right]\left[1-\left(\frac{IADJ}{Ip}\right)\left(1-\frac{tj}{t}\right)\right]\right\}^{1/2} \tag{4}$$

Where *IA* is anterior count, *IP* is posterior count, the factor *fj* (source self-attenuation correction) represents a correction for the source region attenuation coefficient μj and source thickness *tj*. The expression *e*-μet represents the transmission factor across the patient thickness *t* through the ROI with overall effective linear attenuation coefficient μe. The thickness of the source organ and body thickness at the same level were estimated by acquiring a scaled orthogonal view (e.g., sagittal image) and taking direct measurements from CT slices.

F is a simple geometry-based subtraction technique, applied to correct for the overlying background activity in an attempt to avoid the problems inherent in background ROI definition, especially as there was no uniformity for the nearby tissue uptakes near to source organs, which in turn will degrade the accuracy of background correction. However, the observer drew ROIs carefully around several adjacent areas near to the source organs, as far to find proper approximation throughout for better subtraction compensation. Furthermore, to correct overlapped activity caused by intestinal activity in lower poles of kidneys, the average count per pixel in the adjacent intestinal region was subtracted from the inferior kidney region. No scatter correction and spill out correction were applied.

I*A*/*Ip* is the fraction of geometric mean counts that originates from the ROI, where *IADJ* is the count rate through the patient from a region adjacent to the organ ROI with equal sized area (IADJ adjusted to count/pixel to be compatible with equations). Source thickness *tj* and patient thickness *t* remain as previously defined. Direct patient measurements provide *t* and *tj* obtained from lateral or axial views.

The μ_j for the source organs was derived from the calculated bilinear relationship between the narrow beam linear attenuation coefficient and Hounsfield unit (HU) values at energy levels of 208 and 113 keV, in which a linear

interpolation was created from the results obtained by Brown et al. [12], taking into account gamma ray abundance 6 % for 113 keV energy and 11 % for 208 keV. As a result, ultimate linear attenuation coefficient values applied for source organs based on HU were, if the average HU<0:

$$(\mu \mathrm{j} = 0.13 + 0.000132 \times \mathrm{HU}); \quad (5)$$

$$\mathrm{HU} > 0 (\mu \mathrm{j} = 0.13 + 0.00009555 \times \mathrm{HU})$$

The linear attenuation coefficient μ_i for body thickness excluding source region was assumed to be equivalent to water attenuation coefficient 0.13 and just applied for the thickness equal to t-t_j.

The OLINDA/EXM version 1.1. program was used to calculate absorbed dose of source organs in addition to targeted bone marrow dose from the source organs and remainder of the body taking in consideration biexponential fitting for the activity-time integration as it is shown in Eq. 6:

$$Activity(t) = A \times \exp^{-at} + B \times \exp^{-bt} \quad (6)$$

$$\overline{\mathrm{A}}\mathrm{j} = \int_0^\infty \left\{ \mathrm{Aj(t)} = A \times \exp^{-at} + B \times \exp^{-bt} \right\} dt$$

Where $\bar{A}j$ is the cumulative activity of the source organ.

After selecting the ^{177}Lu radionuclide and adult male anthropomorphic model, total body, liver, and kidney activity percentages were filled in the fitting model which was built up in the OLINDA/EXM program and biexponential fitting was applied to generate residence time (h) for each source organ and remainder of the body in the kinetics input form, kidneys fitting R^2=0.98±0.02, liver R^2=0.997±0.003, total body R^2=0.986±0.01, and blood R^2=0.989±0.01. The organ masses and total body mass were modified automatically in the program using a mass correction factor depending on the linear variation between patient mass and adult male phantom mass entered in the space of "multiply all masses by" available in the program input data.

The right and left parotid glands are not included in the OLINDA/EXM program as a source organ. Therefore, we assumed that the gland has a similar morphology to a sphere. So the absorbed dose of the parotid gland was calculated from unite sphere model density doses, available in the OLINDA/EXM program, in which a linear interpolation created between the volumes and the absorbed dose values (density= 1 g/cm^3) in order to find the optimum dose factor, which in turn would simplify dose calculations for unenclosed volumes.

The MATLAB (MathWorks Inc., Natick, MA, USA) program was used to calculate the cumulative activity originated from effective decay (metabolic and physical clearance) in the parotid gland (interpolate shape-preserving fitting was applied) from time (t=0) until the last acquisition time (t_n= 120 h) plus to the cumulative activity from the physical decay which extends from the last acquisition point to infinity. The residence time τ in the gland was calculated by $\tau = \bar{A}/A_0$, where A_0 is administered activity.

The dimensions of the gland were estimated from direct measurement on CT images. The volume of the parotid gland was calculated by

$$\mathrm{V} = \frac{4}{3} \times \pi \times \frac{(\mathrm{L} \times \mathrm{W} \times \mathrm{T})}{8} \quad (8)$$

Where L is the length of the gland, W is the width of the gland, and T is the thickness of the gland

The bone marrow self-dose was also calculated from blood samples using the blood-based model published by Wessels et al. [13]. The functions below clarify the model:

$$\mathrm{DRm} = \overline{\mathrm{A}}\mathrm{bl} \times \frac{0.19}{1-HCT} \times \frac{1.5}{5.2} \times (S_{RM\text{-}RM})_{\mathrm{MD11}} \times \frac{70Kg}{M\mathrm{WB}-patient} \quad (9)$$

$$\overline{\mathrm{A}}bl = \int_0^\infty \left\{ \mathrm{Abl(t)} = A \times \exp^{-at} + B \times \exp^{-bt} \right\} dt \quad (10)$$

Where $\bar{A}BM$ is cumulative activity in bone marrow, HCT is hematocrit and was obtained from a medical laboratory, and $\bar{A}bl$ is cumulative activity in blood. The area under the curve of blood time-activity integration was calculated by the MATLAB program by applying biexponential fitting with paying attention that the standard values of the male phantom published by MIRD schema were used (marrow mass 1.12 kg, phantom weight 73.7 kg $(S_{RM\text{-}RM})_{\mathrm{MD11}}$=1.19E-05 mGy/MBq.S).

Statistical analysis

All results were expressed as mean±SD. For statistical analysis dedicated statistical software was used (StatPlus:mac v5. AnalystSoft Inc., Vancouver, BC, Canada). Wilcoxon test was used to compare different groups. A p value lower than 0.05 was considered as significant

Results

Patients were followed for 24 h after infusion of radiopharmaceutical within 15 min. All patients tolerated the procedure very well and we did not observe any side effects. We did not observe any change in blood pressure, heart rate, or body temperature. In whole-body images obtained 4 h p.i., there was high blood pool and soft tissue uptake. Due to rapid clearance from the blood, images obtained later revealed intense radiotracer uptake at the physiological uptake sites and at the sites of tumor lesions as well (Fig. 1). The radiotracer uptake decreased substantially in images obtained at 120 h p.i.

The blood time-activity curve showed a biexponential clearance curve. The half-life of the distribution phase was

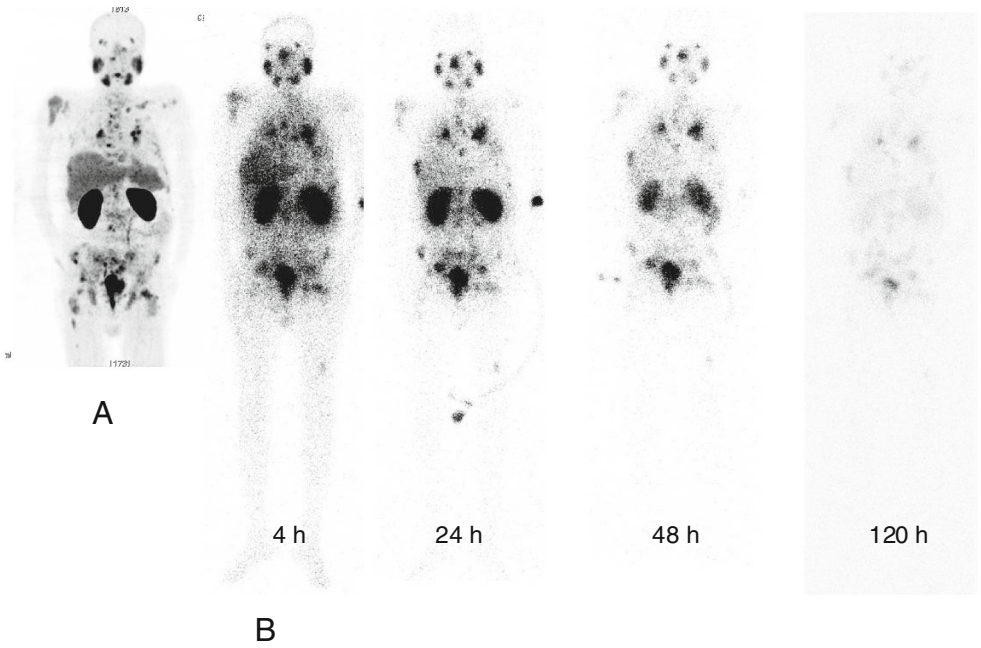

Fig. 1 ^{68}Ga-DKFZ-PSMA-11 PET/CT maximum intensity projection image of a patient (**a**) and ^{177}Lu-DKFZ-617 whole-body images (**b**) obtained at different time intervals

calculated to be 17.5±11.7 min and the half-life of the elimination phase was calculated to be 10.2±5.3 h. Total body residence time showed great variation among patients and it ranged from 24.6 to 62.0 h with a mean value of 37.9±14.6 h (Table 1).

The calculated radiation-absorbed doses for each organ showed great variance among patients. The highest radiation estimated doses were calculated for parotid glands and kidneys. Calculated radiation-absorbed doses per megabecquerel were 1.17±0.31 mGy for parotid glands. For the kidneys the calculated absorbed dose was 0.88±0.40 mGy. The radiation dose given to the bone marrow was significantly lower than those of kidney and parotid glands ($p<0.05$). The calculated radiation dose to bone marrow was 0.03±0.01 mGy/MBq (Table 1).

The estimated maximum safe doses, which did not exceed radiation-absorbed dose constraints for parotid glands, kidneys, and bone marrow, were calculated to be 27.2±6.9, 30.3±11.5, and 65.9±23.7 GBq, respectively (Table 2).

Discussion

The basic principle of radionuclide therapy is to give a high radiation-absorbed dose to the target tissue without producing toxic effects in healthy tissues. However, in radionuclide therapy usually the administered radioactivity is given as a fixed amount or based on body weight or body surface area. A prerequisite for a fixed amount of radionuclide therapy is experience that the therapy is safe and effective as in the case of ^{131}I therapy for the treatment of thyroid cancer. However, to our knowledge, there are no published data regarding the radiation-absorbed dose given to the normal tissues for the systemic therapy with ^{177}Lu-PSMA-617.

Because of large variability of tumor and organ uptake between patients, accurate and reliable absorbed dose estimation is needed for each patient to achieve a maximum dose delivered to the tumor while remaining within acceptable levels in doses delivered to critical organs. It is possible to calculate individual organ and tumor doses precisely during external beam radiotherapy planning. However, the dosimetric calculations for radionuclide therapy are more complex and require the knowledge of in vivo biodistribution and biokinetics of the radiopharmaceutical [14, 15]. Therefore, in order to determine before therapy the amount of radioactivity to administer, a tracer amount of radionuclide is given to the patients and quantitative imaging at different time points is performed to understand the biokinetics of ^{177}Lu-PSMA-617.

First human biodistribution studies of ^{68}Ga-PSMA-11 have demonstrated that highest uptake of radiotracer is observed in kidneys and salivary glands and moderate uptake in liver, spleen, and small intestines, and some uptake in large intestines [6, 8]. So, although the ^{177}Lu-labeled counterpart of the ^{68}Ga-labeled PSMA ligand is not the same compound, we assumed a similar biodistribution pattern due to PSMA expression in normal tissues and we assumed kidneys, parotid glands, and bone marrow as dose-limiting organs to protect.

Bone marrow absorbed dose is one of the major factors limiting the amount of radiopharmaceutical administered to the patient. To avoid bone marrow toxicity, a maximum of 2 Gy of radiation-absorbed dose is generally accepted. From our data the amount of radiation-absorbed dose given to the bone marrow is 0.03±0.01/MBq and it seems that it is safe to administer up to a mean of 65 GBq of ^{177}Lu-PSMA-617.

Table 2 Maximum amount of radioactivity (GBq) to reach radiation-absorbed dose limits

Patient	Parotid gland (30 Gy)	Kidney (23 Gy)	Bone marrow (2 Gy)	Liver (32 Gy)	Total Body (2 Gy)
1	18.1	30.4	79.6	116.4	41.2
2	31.1	13.8	41.9	69.7	21.4
3	31.8	23.5	54.2	137.6	34.6
4	20.3	44.0	95.7	126.3	57.0
5	28.0	33.2	34.3	95.0	20.3
6	24.0	22.4	66.0	142.4	34.9
7	37.5	44.9	89.7	181.3	56.2
Mean	27.2	30.3	65.9	124.1	37.9
SD	6.9	11.5	23.7	35.7	14.8

Organ radiation-absorbed dose constraints in parentheses

These results are comparable with those of ^{117}Lu-DOTATATE treatment. The calculated bone marrow radiation-absorbed doses with ^{177}Lu-DOTATATE have been reported to range from 0.03 to 0.07 mg/MBq [16–18]. The factors that may affect the radiation dose to bone marrow are impairment of renal function or mechanical obstruction of the urinary tract, tumor load, and presence of bone metastases [18, 19]. Accordingly it showed substantial variance among patients ranging from 34.3 to 95.7 GBq, and highest radiation doses were observed in patients who had extensive bone metastases and mechanical obstruction due to extensive disease in the prostate gland (patients 2, 3, and 5). It has been shown that total body residence time increases in patients with decreased renal function and high tumor burden and correlated with bone marrow toxicity during ^{177}Lu-DOTATATE therapy [18–20]. In accordance with these results, we observed the longest residence time in patients who had extensive bone metastases and decreased urinary excretion function due to mechanical urinary obstruction (patients 2, 3, and 5). However, bone marrow dose estimation in patients with prostate cancer who have extensive bone metastases using blood-based dosimetry models would underestimate the absolute dose due to the existence of high avid lesions which increase the dose delivered to bone marrow. Moreover, end-stage prostate cancer patients are extensively treated with chemotherapy and radiotherapy, which may potentially increase the risk of development of hematotoxicity even with a lower amount of radiation dose to the bone marrow.

The kidneys are expected to be dose-limiting organs due to high radiotracer uptake. Based on the earlier experience obtained from conventional external beam radiotherapy, the amount of 23 Gy maximum kidney dose is generally accepted. In order to reach this dose limit to the kidneys a mean of 30 GBq of ^{177}Lu-PSMA-617 can be given. This amount of activity is perfectly correlated with the radioactivity amount found for ^{177}Lu-DOTATATE treatment, which was found to be 33.3 GBq [21]. Conditions that may affect renal function and increase radiation-absorbed dose to the kidneys have been suggested to be older age, prior chemotherapy, and accompanying diseases such as diabetes and hypertension [19, 20, 22]. Accordingly, the amount of radiation-absorbed dose given to the kidneys showed a considerable difference ranging from 13.8 to 44.9 GBq due to individual differences in disease state and renal function between patients. On the other hand, maximum tolerated radioactivity derived from our study should be interpreted cautiously, since 2D-based renal dosimetry overestimates kidney dose in comparison to 3D methods due to overlapping abdominal organ radioactivity accumulation [23].

Although salivary glands contain highly differentiated cells and their proliferation rate is slow, they are exceptionally radiosensitive organs [24]. Salivary gland damage and development of xerostomia is a frequent side effect of radiation therapy, which decreases patients' quality of life [25]. The dosimetric studies have demonstrated that there is a significant extent of damage when radiation dose increases [26]. Damage to the salivary gland reaches a maximum level above doses of 45 Gy. On the other hand, patients receiving less then 30 Gy gradually recover completely within 2 years. Salivary glands are also dose-limiting organs in patients with thyroid cancer who are treated with radioiodine [27]. Although salivary gland dysfunction is a common finding in patients treated with radioiodine, it is usually transient and persistent dysfunction has been reported to be only in 5 % of patients [28]. In our study the maximum amount of ^{177}Lu-PSMA-617 that can be given to reach 30 Gy radiation-absorbed dose is calculated to be 27 GBq and again it showed considerable variation among patients, ranging from 18 to 38 GBq. We do not have an explanation for this variance. Systemic diseases like diabetes mellitus or hypertension or many pharmaceuticals may affect the function of salivary glands [29]. However, there is no information about the PSMA expression and its relation with these conditions.

We are aware of the limitations of individual dose estimations in radionuclide therapy. The in vivo radiopharmaceutical distribution in space and time is subject to change and quantification on scintigraphy affected by many factors, so the

estimation of activity at each time points is possibly subject to large errors up to tens of percentages. For instance, we did not perform scatter correction due to low count acquisition, which may lead to overestimation of calculated organ doses. The error caused by uncertainty of fit function, which was not calculated for this study, also increases the overall calculation errors [30]. Moreover, individual absorbed dose calculations show substantial variations according to the methodologies used [31]. In this study lower radioactivity dose and correspondingly lower amount of PSMA enzyme inhibitor was injected into the patients and we assumed that this amount of radiotracer biologically behaves similarly with a therapeutic dose of radiotracer due to having the same specific activity. However, different amounts of PSMA enzyme inhibitors and doses may have different distribution patterns with different retention times in PSMA-positive and PSMA-negative normal organs and tumors [32]. So the results presented here should be interpreted cautiously. However, this study was carried out in accordance with the published guidelines [23, 33].

In conclusion, ^{177}Lu-PSMA-617 therapy seems to be a safe method for the therapy of castration-resistant prostate cancer patients. Its biokinetic and organ dosimetry results resemble ^{177}Lu-DOTATATE. The maximum tolerated dose of a single dose might be in the dimension of 7.4–11.1 GBq and might depend on tumor involvement of the bone marrow. The maximum cumulative activity should be in the dimension of 30 GBq using kidneys as dose-limiting organ. The fractionation regime that enables the longest duration of tumor control and/or survival will have to be developed in further studies. However, it shows substantial difference among patients, especially in patients with high tumor load and low renal function. Therefore, a patient-specific dosimetric approach should be applied before the therapy to prevent organ toxicity.

Compliance with ethical standards

Funding This study was not funded

Conflicts of interest None.

Ethical approval The study was approved by the local Ethics Committee and was carried out in accordance with the 1964 Declaration of Helsinki.

Informed consent Informed consent was obtained from all individual participants included in the study

References

1. Wright GL, Haley C, Beckett ML, Schellhammer PF. Expression of prostate-specific membrane antigen in normal, benign, and malignant prostate tissues. Urol Oncol 1995;1:18–28.
2. Perner S, Hofer MD, Kim R, Shah RB, Li H, Möller P, et al. Prostate-specific membrane antigen expression as a predictor of prostate cancer progression. Hum Pathol 2007;38:696–701.
3. Silver DA, Pellicer I, Fair WR, Heston WD, Cordon-Cardo C. Prostate-specific membrane antigen expression in normal and malignant human tissues. Clin Cancer Res 1997;3:81–5.
4. Eder M, Schäfer M, Bauder-Wüst U, Hull W-E, Wängler C, Mier W, et al. 68Ga-complex lipophilicity and the targeting property of a urea-based PSMA inhibitor for PET imaging. Bioconjug Chem 2012;23:688–97.
5. Eder M, Schäfer M, Bauder-Wüst U, Haberkorn U, Eisenhut M, Kopka K. Preclinical evaluation of a bispecific low-molecular heterodimer targeting both PSMA and GRPR for improved PET imaging and therapy of prostate cancer. Prostate 2014;74:659–68.
6. Afshar-Oromieh A, Malcher A, Eder M, Eisenhut M, Linhart HG, Hadaschik BA, et al. PET imaging with a [68Ga]gallium-labelled PSMA ligand for the diagnosis of prostate cancer: biodistribution in humans and first evaluation of tumour lesions. Eur J Nucl Med Mol Imaging 2013;40:486–95.
7. Afshar-Oromieh A, Avtzi E, Giesel FL, Holland-Letz T, Linhart HG, Eder M, et al. The diagnostic value of PET/CT imaging with the (68)Ga-labelled PSMA ligand HBED-CC in the diagnosis of recurrent prostate cancer. Eur J Nucl Med Mol Imaging 2015;42:197–209.
8. Kabasakal L, Demirci E, Ocak M, Akyel R, Nematyazar J, Aygun A, et al. Evaluation of PSMA PET/CT imaging using a 68Ga-HBED-CC ligand in patients with prostate cancer and the value of early pelvic imaging. Nucl Med Commun 2015;36:582–7.
9. Kratochwil C, Giesel FL, Eder M, Afshar-Oromieh A, Benešová M, Mier W, et al. [(177)Lu]Lutetium-labelled PSMA ligand-induced remission in a patient with metastatic prostate cancer. Eur J Nucl Med Mol Imaging 2015;42:987–8.
10. Benešová M, Schäfer M, Bauder-Wüst U, Afshar-Oromieh A, Kratochwil C, Mier W, et al. Preclinical evaluation of a tailor-made DOTA-conjugated PSMA inhibitor with optimized linker moiety for imaging and endoradiotherapy of prostate cancer. J Nucl Med 2015;56:914–20.
11. Siegel JA, Thomas SR, Stubbs JB, Stabin MG, Hays MT, Koral KF, et al. MIRD pamphlet no. 16: techniques for quantitative radiopharmaceutical biodistribution data acquisition and analysis for use in human radiation dose estimates. J Nucl Med 1999;40:37S–61S.
12. Brown S, Bailey DL, Willowson K, Baldock C. Investigation of the relationship between linear attenuation coefficients and CT Hounsfield units using radionuclides for SPECT. Appl Radiat Isot 2008;66:1206–12.
13. Wessels BW, Bolch WE, Bouchet LG, Breitz HB, Denardo GL, Meredith RF, et al. Bone marrow dosimetry using blood-based models for radiolabeled antibody therapy: a multiinstitutional comparison. J Nucl Med 2004;45:1725–33.
14. Thierens HM, Monsieurs MA, Bacher K. Patient dosimetry in radionuclide therapy: the whys and the wherefores. Nucl Med Commun 2005;26:593–9.
15. Glatting G, Bardiès M, Lassmann M. Treatment planning in molecular radiotherapy. Z Med Phys 2013;23:262–9.
16. Wehrmann C, Senftleben S, Zachert C, Müller D, Baum RP. Results of individual patient dosimetry in peptide receptor radionuclide therapy with 177Lu DOTA-TATE and 177Lu DOTA-NOC. Cancer Biother Radiopharm 2007;22:406–16.
17. Kwekkeboom D, Bakker W, Kooij P, Konijnenberg M, Srinivasan A, Erion J, et al. [177 Lu-DOTA0,Tyr3]octreotate: comparison with [111In-DTPA0]octreotide in patients. Eur J Nucl Med 2001;28:1319–25.
18. Forrer F, Krenning EP, Kooij PP, Bernard BF, Konijnenberg M, Bakker WH, et al. Bone marrow dosimetry in peptide receptor radionuclide therapy with [177Lu-DOTA(0),Tyr(3)]octreotate. Eur J Nucl Med Mol Imaging 2009;36:1138–46.

19. Svensson J, Berg G, Wängberg B, Larsson M, Forssell-Aronsson E, Bernhardt P. Renal function affects absorbed dose to the kidneys and haematological toxicity during 177Lu-DOTATATE treatment. Eur J Nucl Med Mol Imaging 2015;42:947–55..
20. Sandström M, Garske U, Granberg D, Sundin A, Lundqvist H. Individualized dosimetry in patients undergoing therapy with (177)Lu-DOTA-D-Phe(1)-Tyr(3)-octreotate. Eur J Nucl Med Mol Imaging 2010;37:212–25.
21. Van Essen M, Krenning EP, Kam BLR, de Jong M, Valkema R, Kwekkeboom DJ. Peptide-receptor radionuclide therapy for endocrine tumors. Nat Rev Endocrinol 2009;5:382–93.
22. Sandström M, Garske-Román U, Granberg D, Johansson S, Widström C, Eriksson B, et al. Individualized dosimetry of kidney and bone marrow in patients undergoing 177Lu-DOTA-octreotate treatment. J Nucl Med 2013;54:33–41.
23. Lassmann M, Chiesa C, Flux G, Bardiès M, EANM Dosimetry Committee. EANM Dosimetry Committee guidance document: good practice of clinical dosimetry reporting. Eur J Nucl Med Mol Imaging 2011;38:192–200.
24. Deasy JO, Moiseenko V, Marks L, Chao KSC, Nam J, Eisbruch A. Radiotherapy dose-volume effects on salivary gland function. Int J Radiat Oncol Biol Phys 2010;76:S58–63.
25. Grundmann O, Mitchell GC, Limesand KH. Sensitivity of salivary glands to radiation: from animal models to therapies. J Dent Res 2009;88:894–903.
26. Li Y, Taylor JMG, Ten Haken RK, Eisbruch A. The impact of dose on parotid salivary recovery in head and neck cancer patients treated with radiation therapy. Int J Radiat Oncol Biol Phys 2007;67:660–9.
27. Jeong SY, Kim HW, Lee S-W, Ahn B-C, Lee J. Salivary gland function 5 years after radioactive iodine ablation in patients with differentiated thyroid cancer: direct comparison of pre- and postablation scintigraphies and their relation to xerostomia symptoms. Thyroid 2013;23:609–16.
28. Grewal RK, Larson SM, Pentlow CE, Pentlow KS, Gonen M, Qualey R, et al. Salivary gland side effects commonly develop several weeks after initial radioactive iodine ablation. J Nucl Med 2009;50:1605–10.
29. Sreebny LM, Valdini A, Yu A. Xerostomia. Part II: relationship to nonoral symptoms, drugs, and diseases. Oral Surg Oral Med Oral Pathol 1989;68:419–27.
30. Norrgren K, Svegborn SL, Areberg J, Mattsson S. Accuracy of the quantification of organ activity from planar gamma camera images. Cancer Biother Radiopharm 2003;18:125–31.
31. Garkavij M, Nickel M, Sjögreen-Gleisner K, Ljungberg M, Ohlsson T, Wingårdh K, et al. 177Lu-[DOTA0,Tyr3] octreotate therapy in patients with disseminated neuroendocrine tumors: analysis of dosimetry with impact on future therapeutic strategy. Cancer 2010;116:1084–92.
32. Kletting P, Müller B, Erentok B, Schmaljohann J, Behrendt FF, Reske SN, et al. Differences in predicted and actually absorbed doses in peptide receptor radionuclide therapy. Med Phys 2012;39:5708–17.
33. Hindorf C, Glatting G, Chiesa C, Lindén O, Flux G, EANM Dosimetry Committee. EANM Dosimetry Committee guidelines for bone marrow and whole-body dosimetry. Eur J Nucl Med Mol Imaging 2010;37:1238–50.